Inelastic Response of a Long Span Bridge under Asynchronous Near-Field Pulse-Like and Far-Field Excitations

Laleh Yasrebi[1*] and Mohsen Ghafory-Ashtiany[2]

1. Ph.D. Candidate, International Institute of Earthquake Engineering and Seismology (IIEES),
* Corresponding Author; email: lyasrebi@gmail.com
2. Professor, International Institute of Earthquake Engineering and Seismology (IIEES)

Received: 09/09/2014
Accepted: 21/02/2015

ABSTRACT

Due to the spatial variations of the strong ground motions and Near-Field (N-F) effects, significant and unexpected damages have been observed in long-span bridges during past earthquakes. One of the outstanding characteristics of N-F motions is the forward directivity effect seen as a single, intense, long period pulse at the beginning of velocity records in the fault-normal direction. To better understand the effect of this pulse and the wave passage effect of spatially correlated motions on the seismic response of long-span bridges in comparison with these bridges' response to the far-field earthquakes, a comprehensive case study has been done in three parts on the finite element model of a long-span bridge: 1) Uniform excitations of the model bridge with forward directivity pulses and the original records; 2) Asynchronous excitations with different shear wave velocities for impulsive part of the inputs; and 3) Comparison of the wave passage effect of two sets of near-field and far-field strong ground motions (SGMs) on the seismic response of the model bridge. The results show that the wave passage effect of forward directivity N-F pulses can have significant influence on the bridge nonlinear response, and it becomes more evident in the soft soils causing severe seismic demands. Even in the case of rock sites, ignoring this effect can result in under-designed piers. Besides, comparison of the near-field and far-field SGM excitations effect on the bridge response indicates that although in uniform excitations both sets cause approximately the same displacement response values, in the case of asynchronous inputs, the N-F records can produce larger ductility demands.

Keywords:
Asynchronous motions; Wave passage effect; Near-field; Forward directivity; Far-field; Apparent wave velocity; Long span bridge

1. Introduction

The studies and observations from the past earthquakes such as the 1994 Northridge, the 1995 Hyogoken-Nanbu (Kobe) and the 1999 Chi-Chi revealed that the design of extended long-span bridges for uniform strong ground motion (SGM) inputs at piers' supports is not safe and realistic, especially for the near-source excitations where the variability of SGMs with time and spatial position is high [1]. Today, modern design provisions for the structures, such as long span bridges, require accounting for the spatial variation of the earthquake ground motions [2], especially when the supporting piers are far apart and in different geotechnical conditions.

The effect of spatial variation of seismic ground motions (SVEGM) on the response of extended structures was recognized since 1960s [3]. This effect could be attributed to three main mechanisms [4]: 1) The difference in the arrival times of the

seismic waves at different locations commonly known as the "wave passage effect"; 2) The change in shape of the propagating waveforms due to reflections and refractions of waves through the highly inhomogeneous soil medium and the superposition of the waves known as the "geometric incoherence effect"; and 3) Modification of the amplitude and frequency content of the ground motion at different locations on the ground surface due to different local soil conditions known as the "local site effect".

Besides, the complexity of the wave reflections, refractions and superposition that happen as the seismic waves travel through the soil media [5], the nature of the strong ground motions (SGM) close to the rupturing fault can be significantly different from those observed at large distances. In the near-fault zones, SGMs are influenced by the rupture mechanism and slip direction relative to the site, which generate wave radiation directivity and permanent ground displacements [5]. These effects can be divided into fault normal pulses (forward directivity) and fault parallel ramps (or fling step). In addition to the large velocity pulses in both the fault-normal and fault-parallel directions, near-fault motions also tend to exhibit corresponding long period, large amplitude ground displacement pulses [6]. On the other hand, from analytical point of view, under spatially varying support excitations, the response of a bridge can be expressed as the sum of pseudo-static and dynamic components [7]. Considering that, the pseudo-static component is the static response of the bridge (neglecting inertia and damping forces) due to the difference between the adjacent support displacements [7]; it is zero in the case of the uniform excitations (UE) or infinite travelling wave velocity. As the wave velocity decreases, the arrival time of traveling waves from one support to another one increases and consequently the pseudo-static part of response, due to the larger differential displacements of the support points, increases. In the case of near-field excitations which contain strong long period pulses in their displacement records, the growth of the pseudo-static response can be even more pronounced as the result of the wave passage effect.

Past studies has shown that the impulsive ground motions near earthquake faults, specifically the amplitude and period of velocity pulses, have a significant effect on the performance of the structures [8-13]. Due to the limitations of early seismic instrumentation, signal processing schemes adopted a process which filtered strong motion records into a band-passed frequency range. The removal of the low-frequency components caused a significant effect on the ground velocities, where the low frequency velocity pulses were mainly removed. To understand the significance of these types of historically neglected low frequency motions, and how best to incorporate the hazard associated with these motions in future seismic evaluations, the seismic response of long-span bridges to the near-fault motions were investigated using synthetically generated motions [14]. Then, actual measured broadband near-fault ground motions were used to study the effects of low-frequency motions on the response of a long-span suspension cable stayed bridge. The results showed that band-pass filtering of broad-band records, can cause significant underestimation of the deck truss chord forces up to a factor of 2 [15]. Furthermore, the study on the influence of the spatially varying near-source SGMs on the relative response of two bridge frames showed that the assumption of uniform ground excitation in the analysis and design might not provide a realistic estimation of the pounding responses of the bridge frames [16]. Recently, the survey of the effect of the near fault pulse-like ground motions on the seismic demand of Highway Bridges revealed that the characteristics of near-fault pulses and their effect have not been considered in modern design provisions for bridges [17]. Succeeding that, the earthquake response of a three-span, simply supported bridge was investigated to the near-field pulses; concentrating on the drifts of piers [18]. The results showed that the long continuous decks have large inertia, and through their large longitudinal rigidity they force all relative displacements, between the deck and the ground, to be taken by the piers, and the wave-passage effect can lead to an increase of about 25% to 40% in the pier drifts.

So far, most of the studies have been focused on the effects of "spatially variable far-field motions" on the behavior of extended bridges. It was after Northridge, Kobe and Chi-Chi earthquakes that the observations showed the combined effect of "spatial variability" and "near-field SGM" caused excessive seismic demands of long-span bridges (especially with stiff piers); and still there is a lack

of comprehensive simultaneous studies on both subjects. The purpose of this paper as a case study is first to analyze the inelastic response of a stiff long-span pre-stressed bridge under both near-field and far-field asynchronous excitations (the wave passage effect), in the bridge longitudinal direction. The second goal is to compare the corresponding seismic demands with those of synchronous inputs. The near-field records have been selected from a SGM database which consists of a large number of processed broad-band near-field records located in the vicinity of their respective causative faults and from a variety of tectonic zones worldwide, having the forward directivity (FD) effect with distinct pulses in the related velocity records. Besides, a parametric study on the asynchronous long period pulses as the input of nonlinear time history analyses has been done separately, focused on the pulse durations and traveling wave velocities. These pulses are extracted from the original records by Mavroeidis and Papageorgiou's proposed analytical function [6], which will be discussed later. The nonlinear time history responses are presented for the piers' drifts and curvature ductility demands. Of course, this study is much more extensive, including "geometric incoherence effect" of near-field pulse-like motions on a number of different bridge models with some issues related to record simulation discussions, which will be presented in another paper.

2. Equations of Motion for Multi-Support Excitation Problems

To have a brief description of the theoretical background of multiple support excitation problems, and for completeness, the procedure for deriving dynamic equations of motion is summarized here as [19]. For the general case of earthquake excitation, all of the support DOFs should be included in the equations of motion as follows:

$$\begin{bmatrix} M_{ss} & M_{sg} \\ M_{gs} & M_{gg} \end{bmatrix} \begin{Bmatrix} \ddot{x}_s^a \\ \ddot{x}_g \end{Bmatrix} + \begin{bmatrix} C_{ss} & C_{sg} \\ C_{gs} & C_{gg} \end{bmatrix} \begin{Bmatrix} \dot{x}_s^a \\ \dot{x}_g \end{Bmatrix} + \begin{bmatrix} K_{ss} & K_{sg} \\ K_{gs} & K_{gg} \end{bmatrix} \begin{Bmatrix} x_s^a \\ x_g \end{Bmatrix} = \begin{Bmatrix} 0 \\ f_g \end{Bmatrix} \quad (1)$$

in which subscripts *s* and *g* stand for superstructure and support/ground DOFs, and superscript *a* symbolizes absolute coordinate. The support force vector is represented by f_g. For the sake of simplicity, Eq. (1) is formulated in terms of linear structures. However, for nonlinear structures, the stiffness matrix can be state-dependent. The expanded form of the first block row of Eq. (1) is [20]:

$$M_{ss}\ddot{x}_s^a + C_{ss}\dot{x}_s^a + K_{ss}x_s^a = -M_{sg}\ddot{x}_g - C_{sg}\dot{x}_g - K_{sg}x_g \quad (2)$$

and the equations of motion in absolute coordinates for the lumped mass system (in which the coupling terms in the mass matrix are zero) become:

$$M_{ss}\ddot{x}_s^a + C_{ss}\dot{x}_s^a + F_r = -C_{sg}\dot{x}_g \quad (3)$$

where F_r is the restoring force, defined as $F_r = K_{ss}x_s^a + K_{sg}x_g$.

Based on the above formulation, the absolute displacement can be decomposed into two parts:

$$x_s^a = x_{ps} + x_d \quad (4)$$

where x_{ps} is the pseudo-static response caused by differential support movements; while, x_d, is response to dynamic inertial forces induced by support motions. Further, x_{ps} can be obtained by solving the following static equation:

$$\begin{bmatrix} K_{ss} & K_{sg} \\ K_{gs} & K_{gg} \end{bmatrix} \begin{Bmatrix} x_{ps} \\ x_g \end{Bmatrix} = \begin{Bmatrix} 0 \\ f_g \end{Bmatrix} \Rightarrow \quad x_{ps} = -K_{ss}^{-1}K_{sg}x_g = R_v x_g \quad (5)$$

where $R_v = -K_{ss}^{-1}K_{sg}$ is called the influence factor matrix. By substituting Eqs. (4) and (5) into Eq. (3), the equations of motion in relative coordinates change as follows:

$$M_{ss}\ddot{x}_d + C_{ss}\dot{x}_d + K_{ss}x_d = -M_{ss}R_v\ddot{x}_g - (C_{ss}R_v + C_{sg})\dot{x}_g \quad (6)$$

To have a damping force proportional to the relative velocity $\dot{x}_d$, the coupling damping matrix C_{sg} can be set equal to $-C_{ss}R_v$ such that the second term in the RHS of Eq. 6 is equal to zero. Then, Eq. (7) becomes:

$$M_{ss}\ddot{x}_d + C_{ss}\dot{x}_d + K_{ss}x_d = -M_{ss}R_v\ddot{x}_g \quad (7)$$

Solving nonlinear problems are also based on these equations. In nonlinear multi-support-excitation problems, as the total displacement is decomposed into pseudo-static and dynamic components, a

time-stepping integration is required to extract both components (x_{ps} and x_d) throughout the nonlinear analysis (e.g. Newmark-β direct integration method). Besides, by choosing an appropriate hysteretic model, the restoring force F_r of each member can be modeled [20].

The time-history analyses for this study were performed in OpenSees. In this software, the multi-support excitation equations are developed in absolute coordinates as shown in Eq. (2), thus the analysis results at the nodes are in absolute values too. The multi-support load pattern command in OpenSees allows similar or different prescribed ground motions to be the input at various supports in the structure. If only the acceleration time series is provided as the input ground motions, numerical integration is required in the program to determine the velocities and displacements. In this study, the earthquake excitations are described in the form of the displacement time histories.

3. Case Study: The Bridge and Its Finite Element Model

The model bridge that has been used for the numerical analysis has a segmental precast pre-stressed concrete box-girder deck with single piers and free-cantilever construction method as shown in Figure (1). The continuous non-prismatic deck has total length of 200 meters with three spans of 50 m, 100 m and 50 m. The deck is post tensioned with pre-stress forces. The two piers of the bridge are prismatic and have equal height of 15 m with rectangular section dimension of 3 × 4 m^2 with bending reinforcement ratio of $\rho_s = 0.021$ and 0.01 for the longitudinal and transverse directions as shown in Figure (1c). A row of fixed bearings (proposed by Eurocode-8 in the bridges with precast and pre-stressed decks or bridges that are being constructed using the incrementally launching method with tall piers), as a rotation-free connection, is installed on the top of each pier in the transverse direction. The bridge is designed according to the Iranian national bridge design codes for gravity and seismic loads, respectively [21-22]. It is assumed that the transverse reinforcement of the piers provides the adequate seismic shear capacity and the dominant mode of failure is the flexural mode. The specified 28-day concrete compressive strength is $f'_c = 34.5\ MPa$ and the nominal yield strength of the reinforcement steel is $f_y = 414\ MPa$ (ASTM-A706-Grade 60).

In order to investigate the nonlinear behavior of the bridge, a three-dimensional finite element model has been built up in the software framework OpenSees. The 'Nonlinear-Beam-Column' element together with 'Fiber' section is used for modeling of

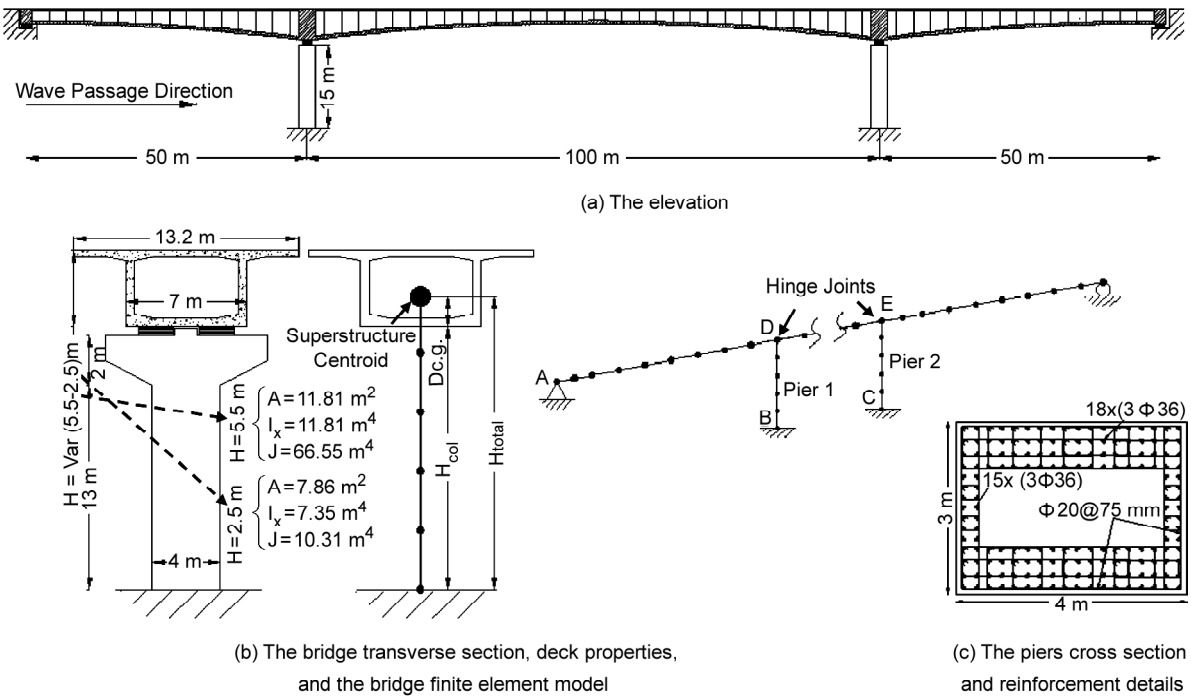

Figure 1. The reference bridge, the finite element model and the details.

piers. This type of element is based on the force formulation and considers the spread of plasticity along the element. In a 'Fiber' section, the stress-strain response of fibers is integrated to determine the resultant behavior of the section. The defined 'aggregator' option in OpenSees was implemented to add constant torsional properties to the pier fiber element sections [23]. For the confined concrete and reinforcement steel properties, the materials 'Concrete02' and 'Steel02' are used in the fiber sections:

"Concrete02" is one of the models available in OpenSees, which can include concrete tensile strength. Based on the PEER recommendation, this strength for both confined and unconfined concrete is included in the nonlinear analysis. The commonly used method to specify the model material properties (expected values) is to amplify the design concrete strength and strain based on Mander's confined concrete model. This constitutive model is suggested by Caltrans to be used for material properties of concrete components [24-25].

"Steel02" is a uniaxial steel material with isotropic strain hardening. It also provides control over the transition from elastic to plastic portions. The strain hardening effect is optional and can be specified in compression or tension. This type of material is widely used for the reinforcement in the RC bridge columns with fiber section properties [26].

The materials property values with their stress-strain relationships are shown in Figure (2). These values are the expected values that are used in this analysis, as it is suggested and calculated according to Caltrans SDC 2004.

It is assumed that due to a large post tensioning force in tendons, the deck will have linear behavior; therefore, it is modeled by three-dimensional 'Elastic-Beam-Column' elements with the maximum cross-section area, bending and torsional moments of inertia on top of the piers and the minimum values in the middle of 100 m span, Figure (1d). The bending stiffness is with no reduction ($I_{eff} = I_g$), as it is recommended for pre-stressed concrete box girder sections by SDC 2004. The deck masses are assigned as translational and rotational lumped masses at the end joints of each linear element. The superstructure elements are placed at the centroid of the non-prismatic deck cross sections. The top of the piers is defined at a distance of Dc.g (difference

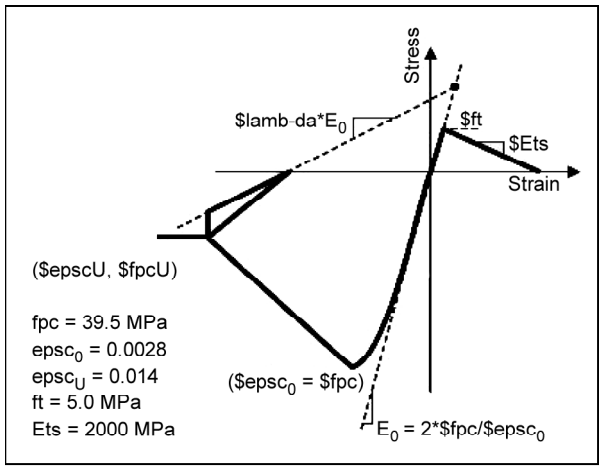

(a) Concrete02 in OpenSees

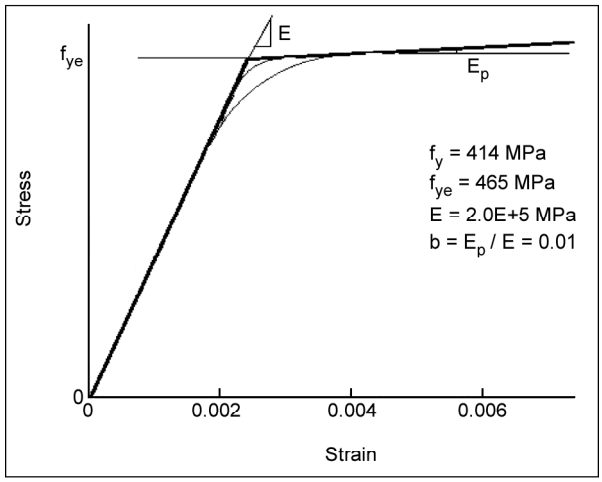

(b) 'Steel02', in OpenSees

Figure 2. The material properties and stress-strain relationships based on Caltrans SDC-2004 for in OpenSees.

between the deck bottom slab and the vertical centroid of the deck cross sections) above the clear height of the bridge column as in Figure (1c), [27]. Besides, the deck connection to the piers is modeled as hinge joints [28]. The pier bases are assumed fixed at the ground level and the abutments in the longitudinal direction, from left to right, are modeled as ideally hinged and roller supports. The viscous Rayleigh damping of 5% and P-Delta effect are also included in the nonlinear analysis of the finite element model. It should be noted that the assumptions made in the modeling; regarding the abutments behavior, the material properties and neglecting soil-structure interaction can affect the analysis results. To obtain more realistic analysis, these points should be considered in the model.

The validity of the finite element model is checked in five stages: 1) a modal analysis is done with

OpenSees and Sap2000 to compare the model's mode shapes and natural frequencies in the two software [29]; 2) to compare the moment-curvature results obtained from a fiber-section and a beam-section analysis, two computer programs (OpenSees and Response-2000) is used [30]; 3) to obtain convergent time history analysis results, with a minimum number of layers in the pier fiber section, a series of moment-curvature section analyses are performed for different number of layers using OpenSees; 4) to obtain an optimum number of integration points along the "Nonlinear-Beam-Column" pier elements, a series of pushover analysis are done for different number of integration points in OpenSees; and 5) to verify the assumption of the linear deck, another model of bridge with "Nonlinear-Beam-Column" deck elements, and inelastic materials for its concrete and steel rebars is considered. Moreover, the exact place of tendons with pre-stressed forces is modeled via joining "Steel02" and "Initial Stress" materials (using "section-aggregator" command). Then the time history analysis is performed to examine the stress level of the deck members' materials.

4. Comparative Nonlinear Time History Analyses

4.1. Synchronous and Asynchronous Excitations, Inputs and Results

Six main scenarios for the nonlinear time history analyses are considered for a comparative study of the wave passage effect (WPE) on the bridge model, subjected to the three different sets of input motions at the bridge fixed supports (nodes A, B and C) in the longitudinal direction as shown in Figure (1a). Here, the soil-structure interaction is neglected, because the goal is to focus only on the nonlinear response of the long-span bridge as a dynamic system in two cases of synchronous and asynchronous excitations. The three input sets are forward directivity long period pulses, original near-field records and original far-field records as listed in Tables (A1), (A2) and (A3) in the Appendix A. For each input set, the uniform excitations (UE) and asynchronous excitations results for the pier maximum drift ratios (the drift ratio is a dimensionless quantity and represents the relative displacement of a column divided by its height) (at the nodes D and E on the top of the piers 1 and 2) and the curvature ductility demands, μ_Ψ, (at the nodes B and C on the bottom of the piers 1 and 2) are compared with each other. Besides, to make a comparison between near-field and far-field wave passage effect on the bridge response, the mean peak response values for each of the six scenarios have been computed.

4.2. Analytical Pulse Model

The records with distinct velocity pulses, caused by forward directivity effect, are considered for the near-field SGM input sets, scenarios No. 2, 4b and 5. Forward directivity (FD) occurs when the fault rupture propagates toward a site with a rupture velocity approximately equal to the shear-wave velocity. In this case, most of the elastic energy arrives coherently in a single, intense and relatively long period pulse at the beginning of the record, representing the cumulative effect of almost all of

Table 1. The list of six main scenarios for the nonlinear time history analyses.

Scenario No	Input Motion	Excitation Type	V_{app}	SGM Database	Comments
1	FD Displacement Pulses	Uniform	-	Table A1	Obtained by Eq. (8) (17 Records)
2	Near-Field SN Displacement Records	Uniform	-	Table A1	17 records
3a	Analytical Displacement Pulse	Asynchronous	500 m/s	Arbitrary Pulses (Tp=1.5 to10sec)	Obtained by Eq. (8)
3b			200 to 2000 m/s	Arbitrary Pulse (Tp=3 sec)	
4a	FD Displacement Pulses	Asynchronous	500 and 2000 m/s	Table A1	Obtained by Eq. (8) 17 records
4b	Near-Field SN Displacement Records	Asynchronous	500 and 2000 m/s		
5a	Near-Field SN Displacement Records	Uniform	-	Table A2	27 Records
5b		Asynchronous	500 m/s		
6a	Far-Field FN Displacement Records	Uniform	-	Table A3	22 records
6b		Asynchronous	500 m/s		

the seismic radiation from the fault. The phenomenon is even more evident when the direction of slip on the fault plane points toward the site as well [31].

To extract the pulses from original records, an analytical model proposed by Mavroeidis and Papageorgiou is used [6]. It is a simple and reliable model, calibrated with a large number of actual near-fault ground-motion records. This model is capable of capturing the impulsive character of near-source recordings both qualitatively and quantitatively. It also has input parameters with a clear physical meaning, to the extent possible, related to physical parameters of the faulting and wave propagation processes. It should be noted that the study of the dynamic structural response using simplified velocity waveforms (e.g., square, triangular, or sinusoidal pulses), although in the right direction, may yield misleading conclusions if the applied pulses do not capture the time history and response spectrum characteristics of the actual near-field records.

The application of multi-support excitation command in OpenSees requires the displacement time histories as input motions. Hence for obtaining the input pulses, the proposed mathematical model for displacement pulse is used as [6]:

$$d(t)=\begin{cases}\dfrac{A}{4\pi f_p}\left[\begin{array}{l}\sin\left[2\pi f_p(t-t_0)+v\right]+\dfrac{1}{2}\dfrac{\gamma}{\gamma-1}\times\\ \sin\left[\dfrac{2\pi f_p(\gamma-1)}{\gamma}(t-t_0)+v\right]+\\ \dfrac{1}{2}\dfrac{\gamma}{\gamma+1}\sin\left[\dfrac{2\pi f_p(\gamma+1)}{\gamma}(t-t_0)+v\right]\end{array}\right]+C,\\ \text{for } t_0-\dfrac{\gamma}{2f_p}\le t\le t_0+\dfrac{\gamma}{2f_p}\end{cases} \quad (8)$$

Parameter A controls the amplitude of the signal, f_p is the frequency of the amplitude-modulated harmonic (or the prevailing frequency of the signal), v is the phase of the amplitude-modulated harmonic (i.e., $v = 0$ and $v=\pm\pi/2$ define symmetric and anti-symmetric signals, respectively), γ is a parameter that defines the oscillatory character (i.e., zero crossings) of the signal (i.e., for small γ the signal approaches a delta like pulse; as γ increases the number of zero crossings increases), and t_0 specifies the epoch of the envelope's peak. Besides, an objective definition of the pulse duration (T_p) is defined compatible with the physical aspects of the phenomenon, as the inverse of the prevailing frequency (f_p) of the signal. The five parameters $(A, \gamma, v, f_p$ and $t_0)$ were obtained by fitting the analytical model Eq. (8), to each of the original records that can be done for any pulse-like record. A set of 17 strike-slip fault-normal SGM components are selected from Mavroeidis and Papageorgiou database as shown in Table (A1). For each of the records, the displacement pulse is calculated from Eq. (8). The displacement time history of six N-F records and their corresponding analytical pulses are shown in Figure (3).

The maximums of the nonlinear time history responses for the drifts and curvature ductility demands of the first two scenarios (the FD pulses and original near-field SGMs uniform excitation analysis) are shown in Figure (4). The inputs for these two analyses are the analytical pulses and the original N-F records of Table (A1). Comparing the analysis results shows that the mean peak value of the drifts and curvature ductility demands for scenario No. 1 are more than 53% of that of scenario No. 2 as shown in Table (2). It can be seen that the FD pulses seem to be an effective part of near-field motions in synchronous excitations of the bridge.

Table 2. The mean peak values of the nonlinear responses (drifts and curvature ductility demands) due to the uniform excitations, scenarios No. 1 and 2.

Response	Mean of Peak Values		Ratio of Mean Values (Scenario No.1/ No.2)
	Scenario No.1	Scenario No.2	
Drift (Pier 1)	0.0011	0.0021	0.53
Drift (Pier 2)	0.0025	0.0044	0.578
μ_ψ (Pier 1)	0.108	0.205	0.53
μ_ψ (Pier 2)	0.252	0.439	0.574

4.3. Apparent Wave Velocity

The variation of ground motions at two distant locations is primarily determined by the wave apparent velocity, V_{app}, which depends on the incident angle of seismic waves into the site and the site condition. A study of the recorded time histories revealed that V_{app} is frequency dependent and quiet irregular. However, without losing generality it can be assumed that the incoming seismic wave consists of the primarily S wave then the lower bound of the V_{app} will be the shear wave velocity of the site (V_s),

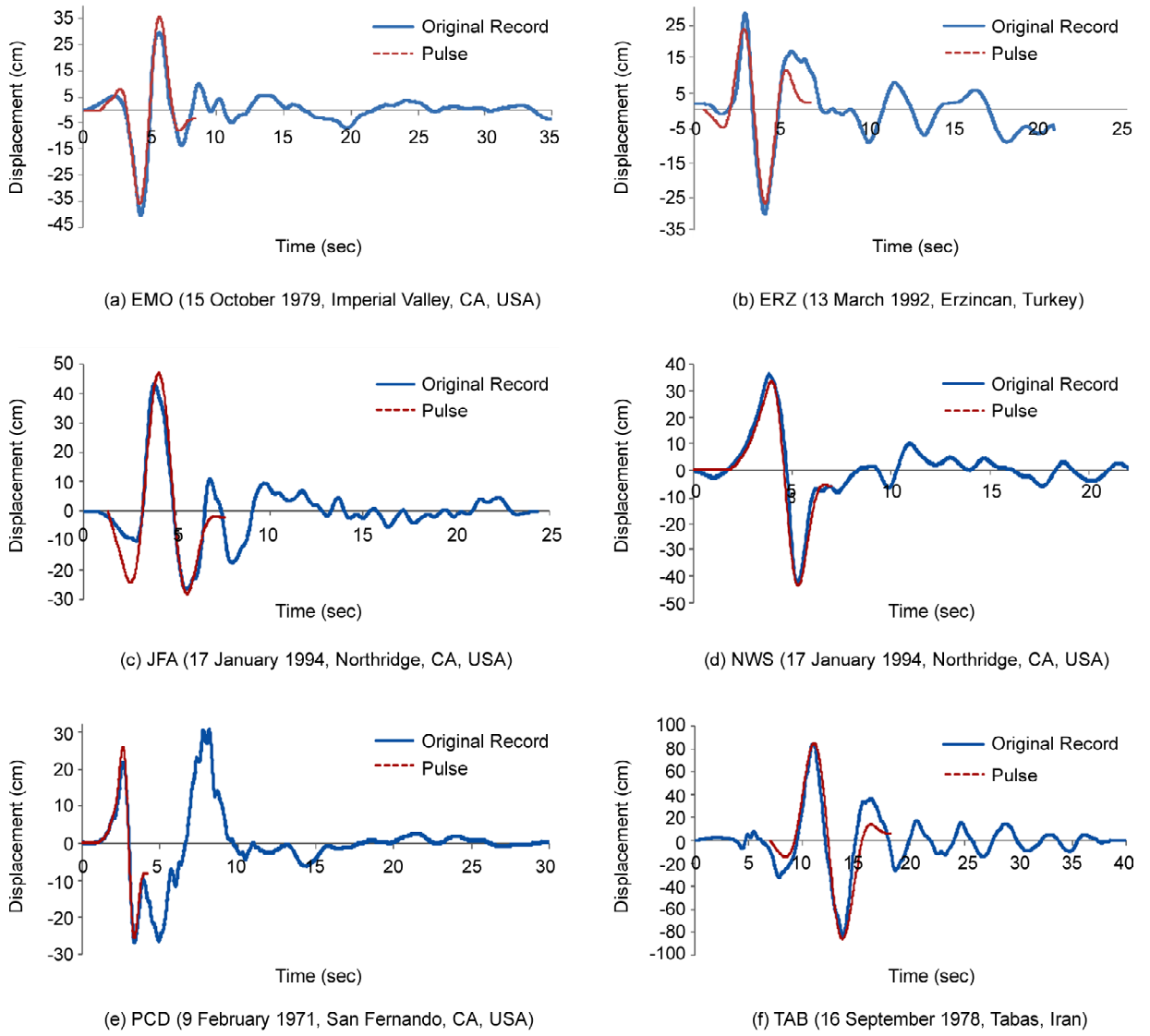

(a) EMO (15 October 1979, Imperial Valley, CA, USA)

(b) ERZ (13 March 1992, Erzincan, Turkey)

(c) JFA (17 January 1994, Northridge, CA, USA)

(d) NWS (17 January 1994, Northridge, CA, USA)

(e) PCD (9 February 1971, San Fernando, CA, USA)

(f) TAB (16 September 1978, Tabas, Iran)

Figure 3. The earthquake displacement time histories at stations EMO, ERZ, JFA, NWS, PCD and TAB (the SN components) and their corresponding analytical pulses, Table (A1).

and the upper bound equals infinity. These two bounds represent horizontally and vertically propagating incident waves into the site [16]. In this study, it is assumed that $V_{app} = V_s$. Since the forward-directivity pulses of near-field motions have their maximum energy in the fault-normal SGM components, it is assumed that the bridge longitudinal axis is aligned with the causative faults normal direction. Besides, to avoid complication in interpreting the analysis results, the input excitation is only applied in the longitudinal direction of the bridge. The excitations are first applied at the left abutment (node A), and there are time lags between the ground motions at other pier supports (nodes B and C). The time lag is calculated as $\Delta t_i = r_i / V_{app}$, where r_i is the separation distance between the left abutment and pier i ($i = 1, 2$).

The FD pulses and original near-field SGMs uniform excitation analysis results (scenarios No. 1 and 2) show that the N-F long period pulses have a significant effect on the bridge peak response values (pier drifts and μ_ψ) in the case of uniform excitations, as shown in Table (2). Scenario No. 3a and 3b (asynchronous excitation with analytical pulses), are defined for a parametric study on the effect of displacement pulse duration (T_p) on the bridge response. In scenario No. 3a an arbitrary form of pulse, derived from Eq. (8), is considered with all parameters fixed except for the prevailing frequency $f_p = 1/T_p$ and the signal amplitude A. The parameter A is adjusted such that with the increase of T_p from 1.5 sec to 10 sec, the maximum

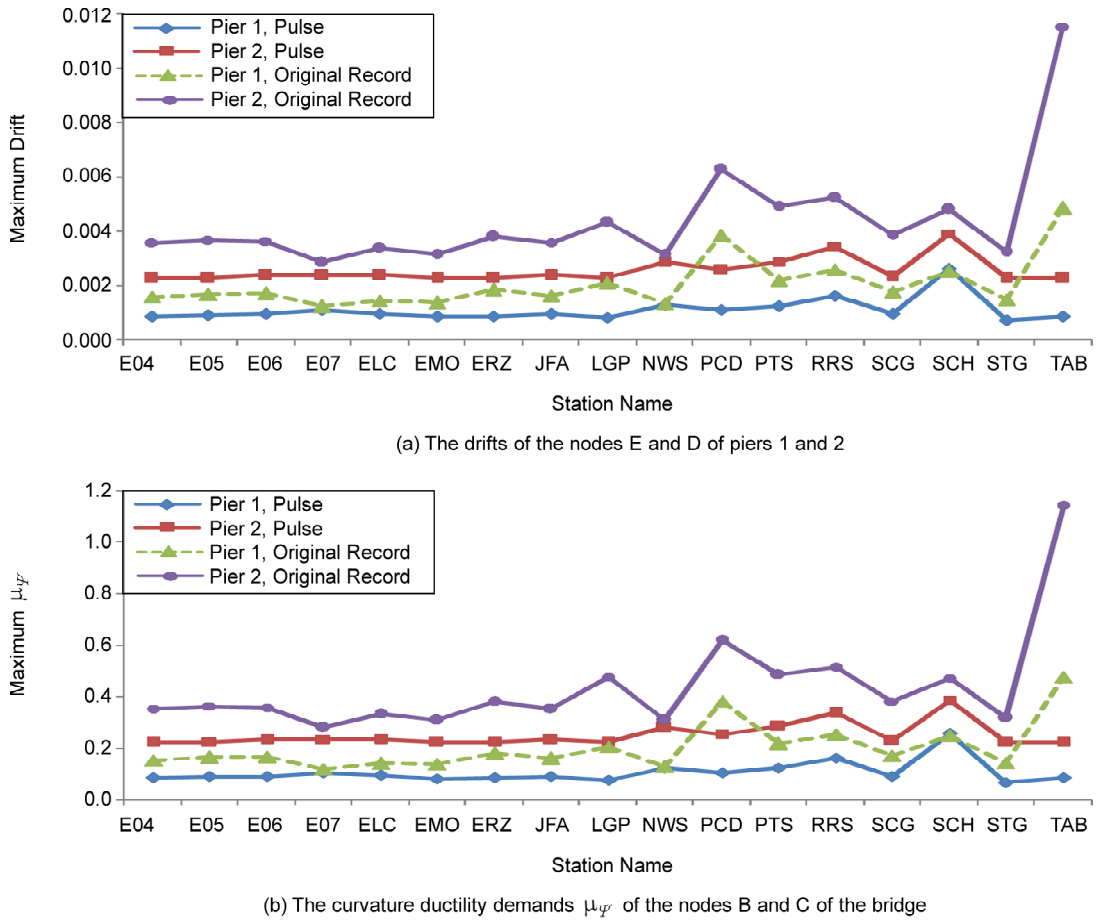

Figure 4. The maximum nonlinear time history responses of the drifts and curvature ductility demands due to UE analysis, scenarios No. 1 and 2 of Table (1).

displacement amplitude of pulse remains fixed as 50 cm. Then, this pulse is set as the asynchronous input of support nodes with $V_s = 500$ m/s. The piers' maximum curvature ductility demands are shown in Figure (5b). It shows that as the pulse duration decreases, the piers seismic demands to asynchronous excitations ascend and this is more evident for pier 2 that is farther from the fixed abutment (at node *A*).

In scenario No. 3b, the pre-mentioned arbitrary pulse period T_p is considered as the average T_p of 17 FD pulses derived from Eq. (9), corresponding to 17 N-F records listed in Table (A1). Then this pulse is considered as the input for asynchronous excitations, in the shear wave velocity range of 200 m/s to 2000 m/s, covering three categories of soft soil, stiff soil and rock sites. The results in Figure (5d) shows that as V_s decreases, the piers' ductility demands and the difference between demands of two piers increase; the latter happens since the participation of pseudo-static component of response is more than the dynamic component in low traveling wave velocities [32], causing a noticeable difference in the adjacent piers' deformations. In this study, the maximum curvature ductility demand for WPE with $V_s = 200$ m/s is more than 6 times higher than that of WPE with $V_s = 2000$ m/s.

The scenarios No. 4a and 4b (asynchronous excitations with FD pulses and original near-field SGMs) are defined to compare the wave passage effect of the corresponding FD pulses of the original N-F records (for $V_s = 500$ and 2000 m/s) with that of the synchronous excitations on the bridge seismic response as shown in Figure (6). As it can be seen in Table (3), the mean maximum nonlinear drifts and μ_Ψ caused by asynchronous pulse inputs with $V_s = 2000$ m/s is more than 60% of that due to asynchronous original N-F records with the same shear wave velocity. This ratio reaches to 70% in the asynchronous excitations with $V_s = 500$ m/s. When these ratios are compared with the corresponding ratio of 53%, related to the synchronous input case (scenarios No. 1 and 2), it can be seen

that the effect of long period near-field pulses would be more severe in case of traveling waves with low shear wave velocities or in soft soil conditions For the case of N-F inputs and hard rock site ($V_s = 2000$ m/s), the mean peak μ_ψ values of piers 1 and 2 are respectively 1.35 and 1.45 times those of the uniform support excitations results. Therefore even in the case of rock sites, the wave passage of near-field motions can considerably increase the seismic demands and ignoring this effect may result in weakly designed bridge piers.

Figure (7) shows the relative displacement time history response at the node D and the bending moment time history response at the node B of pier 1, for synchronous and asynchronous excitations, respectively. The analysis input is the near-field original records of NWS station (1994 Northridge), and STG station (1989 Loma Prieta), and the

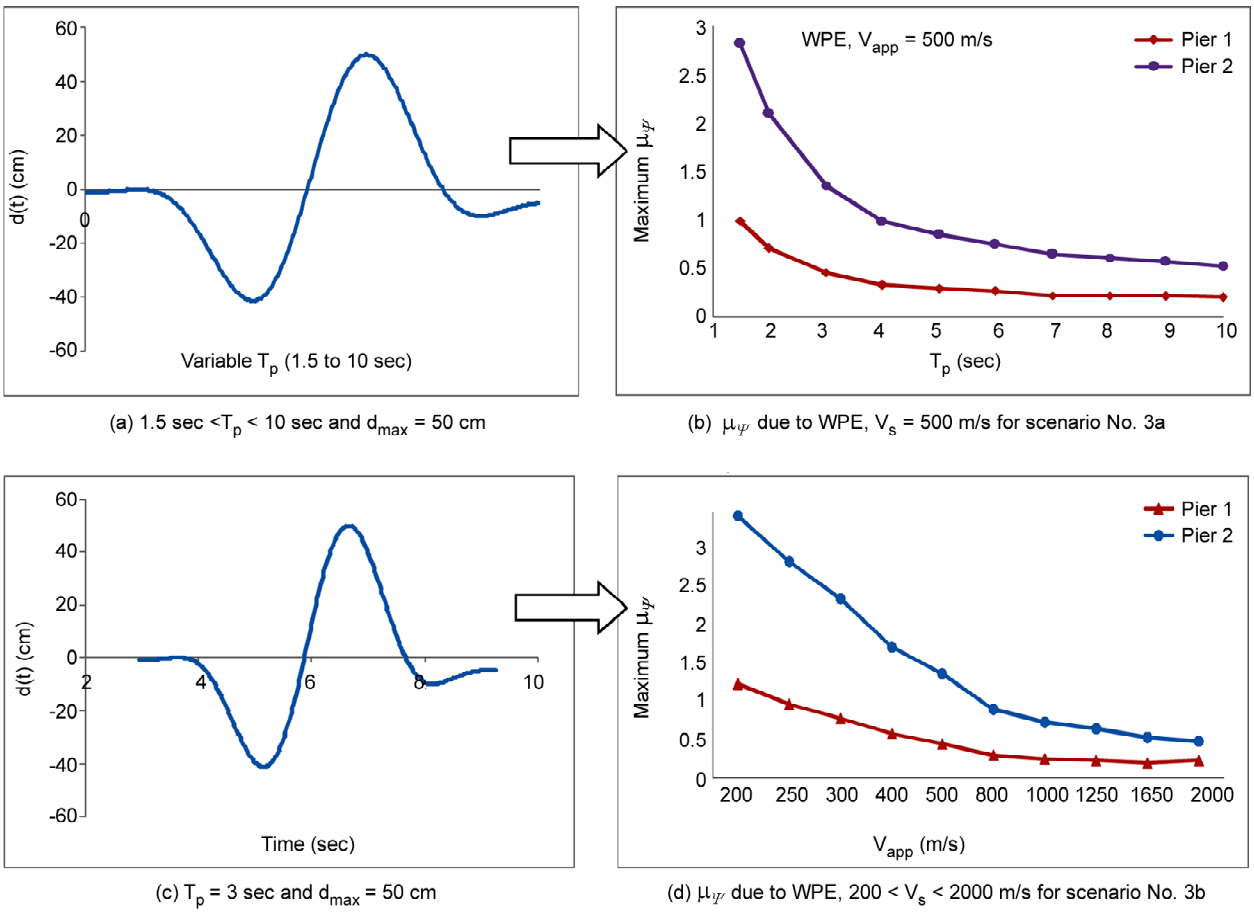

(a) 1.5 sec <T_p < 10 sec and d_{max} = 50 cm

(b) μ_ψ due to WPE, V_s = 500 m/s for scenario No. 3a

(c) T_p = 3 sec and d_{max} = 50 cm

(d) μ_ψ due to WPE, 200 < V_s < 2000 m/s for scenario No. 3b

Figure 5. The displacement time history of the input arbitrary analytical pulses and the piers maximum response of curvature ductility demands to the WPE, scenarios No. 3a and 3b. (a) the pulse for variable T_p, (b) μ_ψ of the nodes B and C, (c) the pulse for a fixed T_p and (d) μ_ψ of the nodes B and C.

Table 3. The average peak response values of nonlinear drifts and μ_ψ for two cases of UE and WPE with inputs: 1) the N-F original records, and 2) the N-F analytical pulses, scenarios No. 4a and 4b.

Scenario No. 4a	Mean of Peak Values			Scenario No. 4b	Mean of Peak Values			Ratio of Mean Peak Values = Response (Pulse)/ Response (N-F Record)			
(Pulse) Response	UE.	WPE V_s =2000m/s	WPE V_s =500m/s	(N-F Record) Response	UE.	WPE V_s =2000m/s	WPE V_s =500m/s				
Drift (Pier1)	0.0011	0.0016	0.0044	Drift (Pier1)	0.0021	0.0025	0.0062	Drift (Pier1)	0.53	0.65	0.71
Drift (Pier2)	0.0025	0.0046	0.0130	Drift (Pier2)	0.0044	0.0064	0.0173	Drift (Pier2)	0.58	0.72	0.75
μ_ψ (Pier1)	0.108	0.1621	0.436	μ_ψ (Pier1)	0.20	0.27	0.62	μ_ψ (Pier1)	0.53	0.60	0.70
μ_ψ (Pier2)	0.252	0.4594	1.286	μ_ψ (Pier2)	0.44	0.64	1.71	μ_ψ (Pier2)	0.57	0.72	0.75

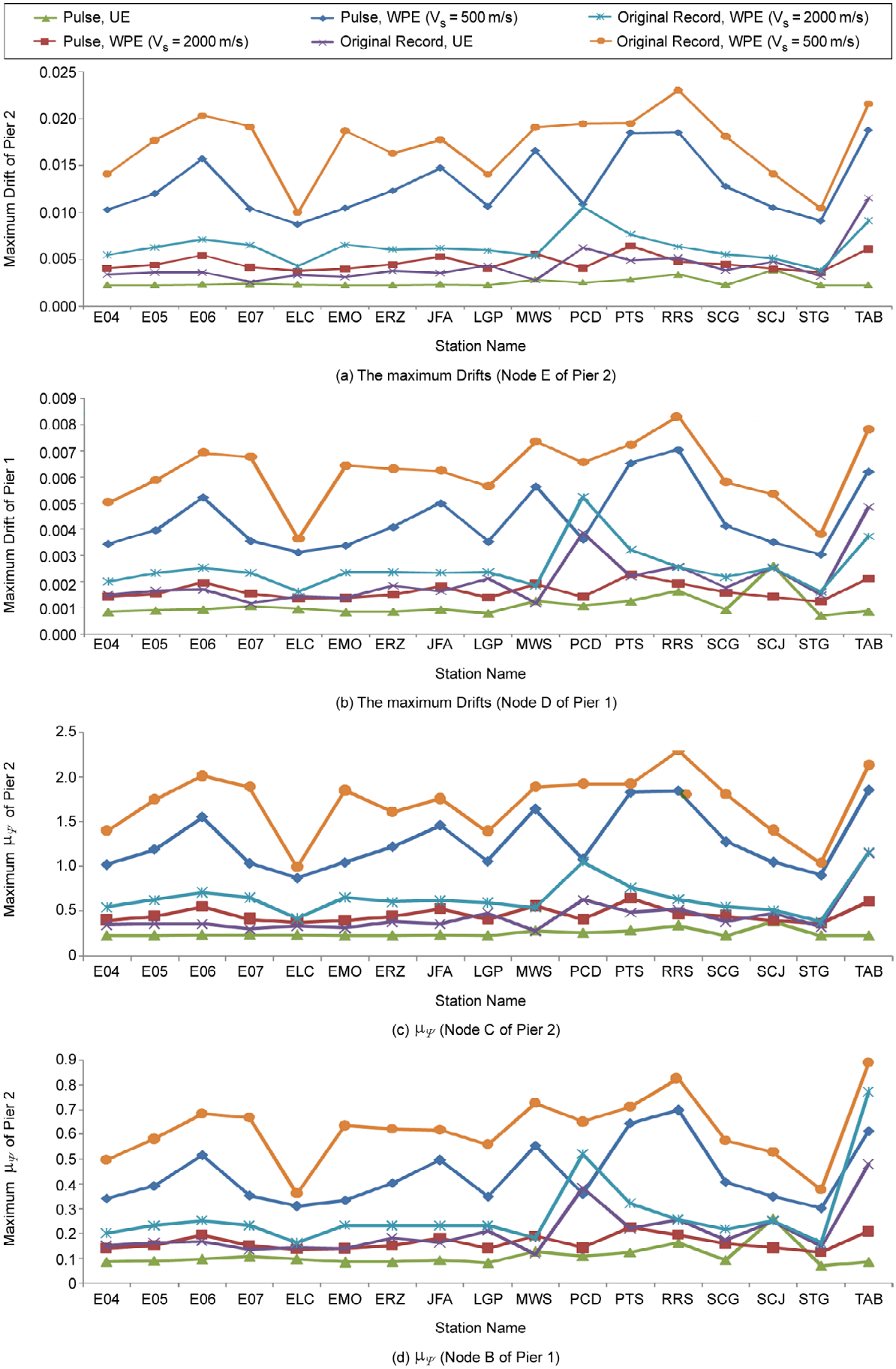

Figure 6. The maximum nonlinear drifts and μ_Ψ for 3 cases of UE, WPE (V_s = 500 m/s) and WPE (V_s = 2000 m/s), with two sets of inputs: 1) the N-F analytical pulses, and 2) the N-F original records, scenarios No. 4a and 4b.

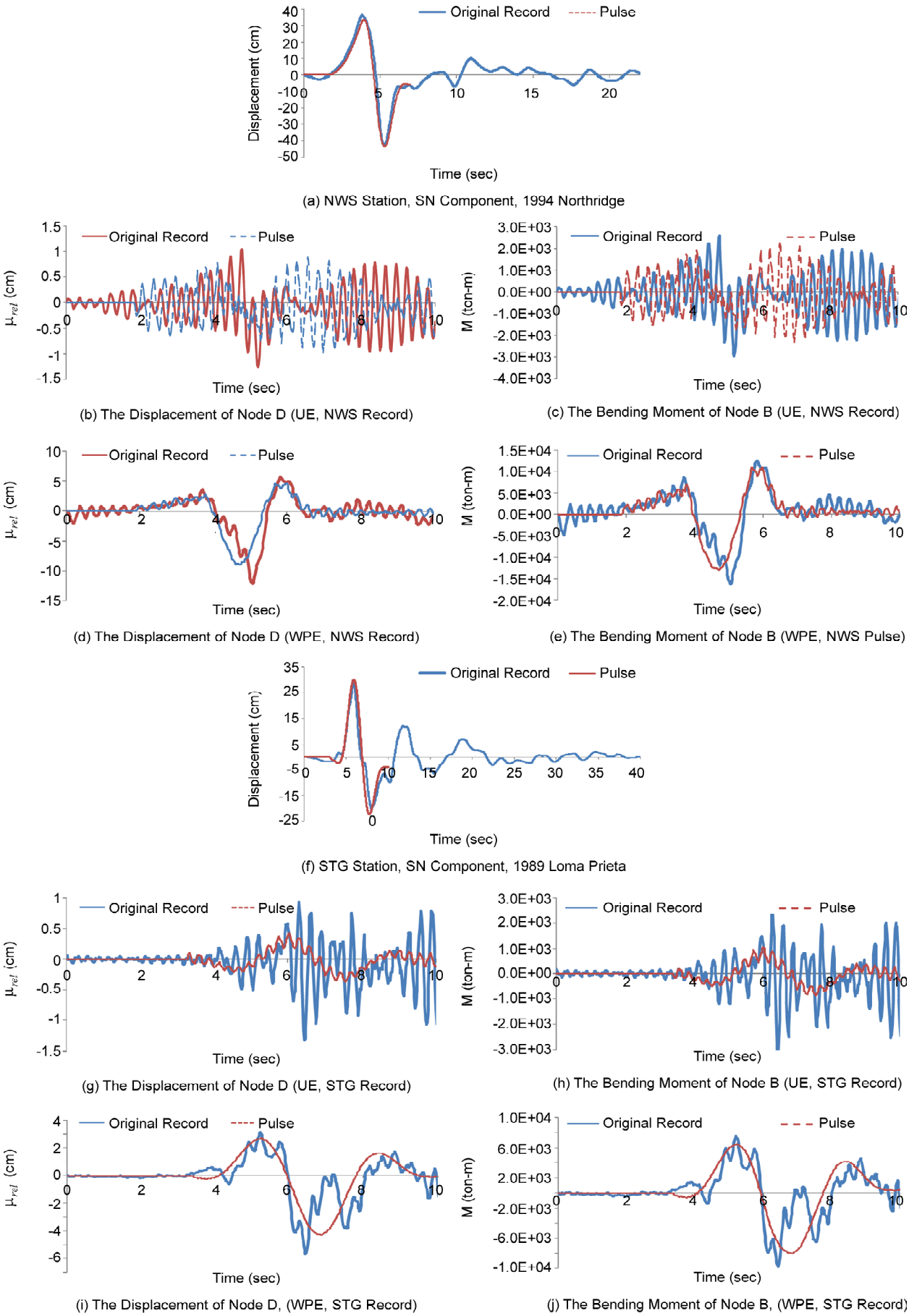

(a) NWS Station, SN Component, 1994 Northridge

(b) The Displacement of Node D (UE, NWS Record)

(c) The Bending Moment of Node B (UE, NWS Record)

(d) The Displacement of Node D (WPE, NWS Record)

(e) The Bending Moment of Node B (WPE, NWS Pulse)

(f) STG Station, SN Component, 1989 Loma Prieta

(g) The Displacement of Node D (UE, STG Record)

(h) The Bending Moment of Node B (UE, STG Record)

(i) The Displacement of Node D, (WPE, STG Record)

(j) The Bending Moment of Node B, (WPE, STG Record)

Figure 7. The displacement time histories of stations NWS of 1994 Northridge EQ, and STG of 1999 Loma Prieta EQ and their analytical pulses as inputs of UE and WPE (V_{app} = 500 m/s), and the corresponding time history responses of the relative displacement and bending moment at the nodes D and B of pier 1 respectively.

corresponding Forward-Directivity pulses extracted from the original record by Eq. (8). For these two records, the wave passage effect of the FD pulses can be a good estimate of WPE in the total record ($V_{app} = 500$ m/s, stiff soil).

Scenarios No. 5a, 5b, 6a and 6b (synchronous and asynchronous excitations with original FD near-field and far-field SGMs) compare the traveling wave effect of far-field SGMs with that of the forward directivity near-field SGMs, on the bridge piers seismic demands. Two sets of PEER-NGA records are considered. The first set contains 27 near-field records with site to source distance $d < 10$ km, Table (A2). The second set consists of 22 far-field records with $d > 10$ km, Table (A3). Both sets have earthquake magnitude in common range of $6.5 < M_w < 7.6$ and average $PGA \approx 0.45$g. Figure (8) shows the peak responses for two cases of uniform and asynchronous excitations with $V_{app} = 500$ m/s; and Table (4) shows the mean peak response values for each scenario case. These results indicate that for the selected far-field database, the mean maximum drift values of pier 1 and 2 for $WPE(V_s = 500$ m/s), are 1.73 and 2.02 times the corresponding values of UE analysis, and the mean maximum curvature ductility demands of pier 1 and 2 for $WPE(V_s = 500$ m/s) are 1.71 and 2.0 times the corresponding values of UE analysis. For the selected near-field database, the mean maximum drift values of pier 1 and 2 for $WPE(V_s = 500$ m/s) are 2.97 and 3.86 times the corresponding values of UE analysis and the average maximum curvature ductility demands of pier 1 and 2 for $WPE(V_s = 500$ m/s) are 2.97 and 3.83 times the corresponding values due to the UE analysis. Therefore, even though the selected strong far-field records produce the UE response values the same as those of near-field records, but the wave passage effect of the near-field FD pulse-like SGMs can produce larger ductility demands in the long-span bridge structures (in this case almost two times larger).

5. Conclusions

The nonlinear time history analyses for the six main scenarios of synchronous and asynchronous excitations and three sets of input motions; as analytical forward directivity long-period pulses, near-field SGMs and far-field SGMs, are performed on a long three span bridge model with stiff piers. To compare the wave passage effect of the three sets of input motion, different values of apparent wave velocity (representing different soil types) is considered for asynchronous excitations. From the results of this case study, including maximum nonlinear drifts and curvature ductility demands of the piers, it can be concluded that:

In the case of the forward directivity near-field uniform excitations, the long period pulses in the

Table 4. The mean peak values of nonlinear time history response of drifts and μ_ψ for two cases of synchronous and asynchronous excitations with the near-field and far-field inputs,Tables (A2) and (A3), scenarios No. 5a, 5b, 6a and 6b.

Scenario No.	Response Component	Average Peak Value
5a N-F Uniform Exc. (27 Records)	Drift (Pier 1)	3.33 cm
	Drift (Pier 2)	7.18 cm
	μ_ψ (Pier 1)	0.185
	μ_ψ (Pier 2)	0.4
5b N-F Asynchronous Exc. (27 Records)	Drift (Pier 1)	9.88 cm
	Drift (Pier 2)	27.7 cm
	μ_ψ (Pier 1)	0.55
	μ_ψ (Pier 2)	1.53
6a F-F Uniform Exc. (22 Records)	Drift (Pier 1)	3.17 cm
	Drift (Pier 2)	6.64 cm
	μ_ψ (Pier 1)	0.175
	μ_ψ (Pier 2)	0.37
6b F-F Asynchronous Exc. (22 Records)	Drift (Pier 1)	5.49 cm
	Drift (Pier 2)	13.42 cm
	μ_ψ (Pier 1)	0.3
	μ_ψ (Pier 2)	0.74

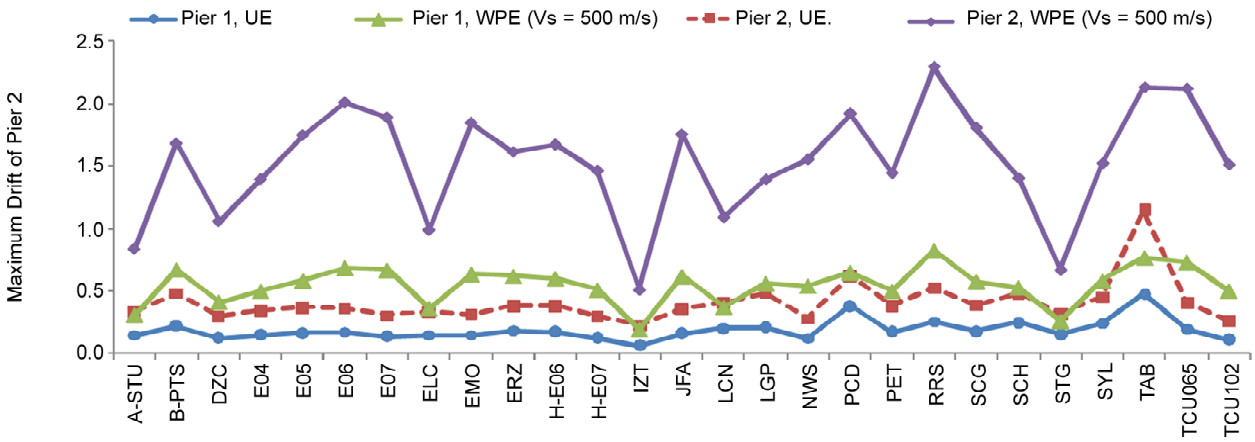

(a) μ_ψ of the Nodes B and C of Piers 1 and 2 for the Near-Field SGMs, Scenarios No. 5a and 5b.

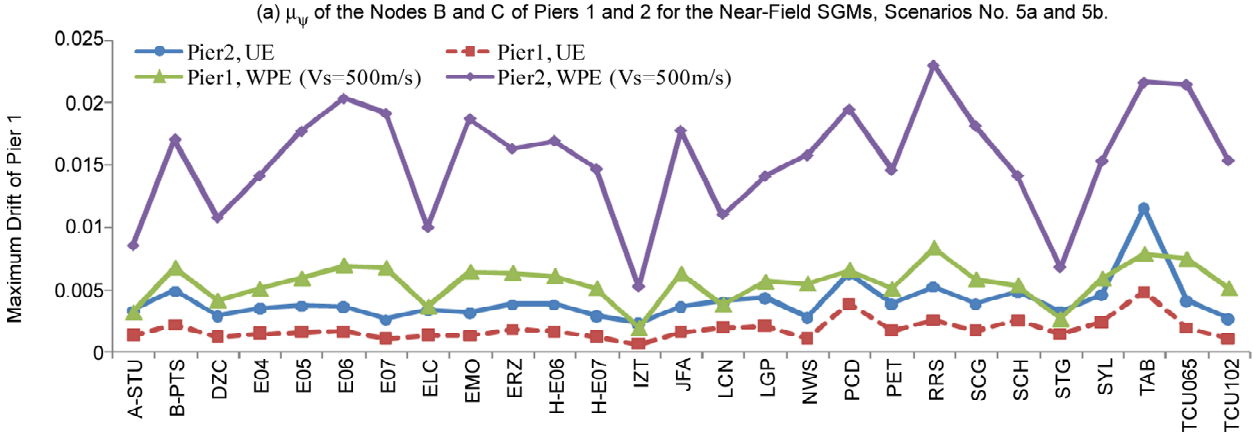

(b) The Drifts of the Nodes D and E of the Bridge for the Near-Field SGMs, Scenarios No. 5a and 5b.

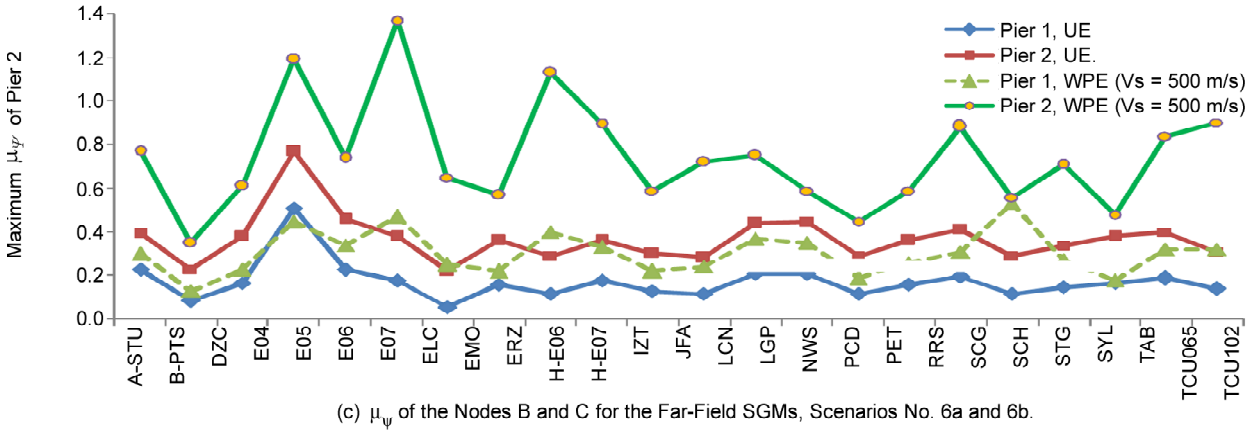

(c) μ_ψ of the Nodes B and C for the Far-Field SGMs, Scenarios No. 6a and 6b.

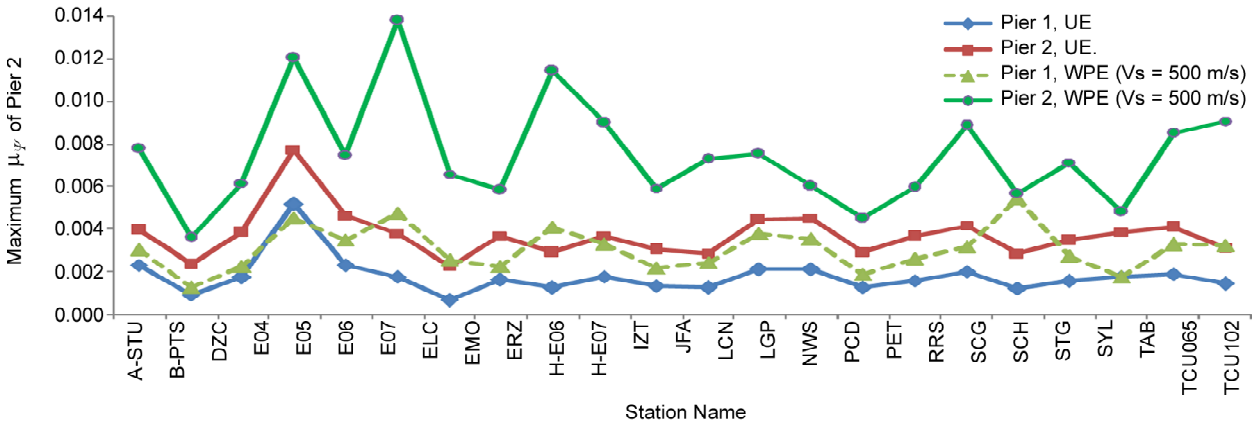

(d) The Maximum Drifts of the Nodes D and E for the Far-Field SGMs, Scenarios No. 6a and 6b.

Figure 8. The maximum nonlinear drifts and curvature ductility demands for the synchronous and asynchronous excitations with the near-field and far-field SGM inputs, Tables (A2) and (A3) for scenarios No. 5a, 5b, 6a and 6b.

input have significant influence on the seismic response. This effect becomes more pronounced in the asynchronous excitations for soft soil sites and the respective high seismic demands shows it is more severe for the piers which are farther from the fixed abutment. Even in the case of the rock sites, where shear wave velocities are high, the wave passage of near-field SGMs could increase the bridge seismic demands to considerable amounts, which if not seen in the seismic design provisions, may result in under-designed piers.

While the bridge seismic response to uniform excitations, due to severe far-field records (with the average PGA values the same as those of near-field records), can be close to the values caused by the near-field inputs; but in the case of asynchronous excitations, the wave passage effect of the near-field FD pulse-like records can produce larger seismic demands in the bridge piers compared with the corresponding far-field seismic demands. Therefore, the wave passage effect, as one out of three main causes of the spatial variability of earthquake ground motions, should be considered in the far-field and near-field excitations of long-span bridge structures with more concentration on the near-field motions that contain forward directivity pulses.

Having more comprehensive results on the effect of spatial variability of near-field motions on long-span bridges' response, also requires the consideration of; 1) the other two SVEGM phenomena known as "geometric incoherence" and "local site effect", which involve record simulation issues, 2) the soil-structure interaction, which can have significant influence on the nonlinear response of long-span bridges; such as introducing flexibility and energy dissipation into the system compared with the assumption of rigid supports, 3) the multi-component (horizontal and vertical *EQ* components) excitations which can excite other vibrational modes and bring about more realistic results, and 4) various configurations of extended bridges with different deck lengths. The effects of these issues, on the nonlinear response of long span pre-stressed bridges, are under study and will be presented in the other papers.

References

1. Shabestari, Kh.T. and Yamazaki, F. (2003) Near-fault spatial variation in strong ground motion due to rupture directivity and hanging wall effects from the Chi-Chi, Taiwan earthquake. *Earthquake Engineering and Structural Dynamics*, **32**, 2197-2219.
2. Earthquake Eng. Research Institute, (1999) *Research Needs Emerging from Recent Earthquakes*. Recommendations from a Workshop Organized by the Earthquake Engineering Research Institute for the National Science Foundation, EERI, San Francisco CA.
3. Bogdanoff, J.L., Goldberg, J.E., and Bernard, M.C. (1961) Response of a simple structure to a random earthquake-type disturbance. *Bulletin of the Seismological Society of America*, **51**, 293-310.
4. Zerva, A. (2009) *Spatial Variations of Seismic Ground Motions: Modeling and Engineering Applications*. Taylor and Francis Group, LLC.
5. Zerva, A. and Zervas, V. (2002) Spatial variation of seismic ground motions: An overview. *Applied Mechanics Reviews*, ASME, **55**(3), 271-297.
6. Mavroeidis, P. and Papageorgiou, A.S. (2003) A mathematical representation of near-fault ground motions. *Bulletin of the Seismological Society of America*, **93**(3), 1099-1131.
7. Clough, R.W. and Penzien, J. (1993) *Dynamics of Structures*. McGraw-Hill, New York.
8. Todorovska, M.I. and Trifunac, M.D. (1997) Amplitudes, polarity and time of peaks of strong ground motion during the 1994 Northridge, California earthquake. *Soil Dynamics and Earthquake Engineering*, **16**(4), 235-258.
9. Hall, J.F., Heaton, T.H., Halling, M.W., and Wald, D.J. (1995) Near-source ground motion and its effects on flexible buildings. *Earthquake Spectra*, **11**(4), 569-605, ISSN 8755-2930.
10. Fenves, G.L. and Ellery, M. (1998) *Behavior and Failure Analysis of a Multiple-Frame Highway Bridge in the 1994 Northridge Earthquake*. Pacific Earthquake Engineering Research Center, University of California, Report No. PEER 98/08.
11. Mylonakis, G. and Reinhorn, A.M. (2001) Yielding oscillator under triangular ground acceleration pulse. *Journal of Earthquake*

Engineering, **5**(2), 225-251.

12. Dicleli, M. (2008) Performance of seismic-isolated bridges with and without elastic-gap devices in near-fault zones. *Earthquake Engineering and Structural Dynamics*, **37**(6), 935-954.

13. Jonsson, M.H., Bessason, B., and Haflidason, E. (2010) Earthquake response of a base-isolated bridge subjected to strong near-fault ground motion. *Soil Dynamics and Earthquake Engineering*, **30**, 447-455.

14. McCallen, D.B., Astaneh-Asl, A., Larsen, S.C., and Hutchings, L.J. (2006) Dynamic Response of the Suspension Spans of the San Francisco-Oakland Bay Bridge. *Proc. of the 100th Anniversary Conf. Commemorating the 1906 San Francisco Earthquake*, EERI, Paper No. 952.

15. McCallen, D.B., Astaneh-Asl, A., Larsen, S.C., and Hutchings, L.J. (2009) *The Response of Long-Span Bridges to Low Frequency, Near-Fault Earthquake Ground Motions*. TCLEE, 1-12.

16. Chouw, N. and Hao, H. (2008) Significance of SSI and non-uniform near-fault ground motions in bridge response I: effect on response with conventional expansion joint. *Engineering Structures*, **30**, 141-153.

17. Dolati, A., Taghikhany, T., and Rahai, A. (2012) Seismic demands of the case study highway bridge under near fault pulse-like ground motion. *15th World Conference on Earthquake Engineering*, Lisbon, Portugal.

18. Jalali, R.S., Bahari Jokandan, M., and Trifunac, M.D. (2012) Earthquake response of a three-span, simply supported bridge to near-field pulse and permanent-displacement step. *Soil Dynamics and Earthquake Engineering*, **43**, 380-397.

19. Chopra, A.K. (2001) *Dynamics of Structures: Theory and Applications to Earthquake Engineering*. 2nd Ed., Prentice Hall, Upper Saddle River, NJ.

20. Li, J., Spencer, B., Jr., Elnashai, A., and Phillips, B. (2012) Substructure hybrid simulation with multiple-support excitation. *Journal of Engineering Mechanics*, ASCE, **138**(7), 867-876.

21. *The Iranian Code of "The Analysis and Design of Concrete Bridges"*. Publication No.389, Appendix to Iranian Concrete Code of Practice for Analysis and Design of Building Structures.

22. *The Iranian code of "Practice for Road and Railway Bridges Seismic Resistant Design"*, Publication No.463.

23. Mazzoni, S., McKenna, F., Scott, M.H., and Fenves, G.L. (2006) *OpenSees Command Language Manual: An Open System for Earthquake Engineering Simulation*.

24. Huang, X. (2012) *Applicability Criteria of Fiber-Section Elements for the Modeling of RC Columns Subjected to Cyclic Loading*. University of Toronto.

25. Caltrans SDC (2004) *Caltrans Seismic Design Criteria*, Version 1.3, California Department of Transportation, Sacramento, California.

26. Sadrossadat Zadeh, M. and Saiidi, M.S. (2007) *Pre-test Analytical Studies of NEESR-SG 4-Span Bridge Model Using OpenSees*. University of Nevada, Reno.

27. Aviram, A., Mackie, K.R., and Stojadinovi, B. (2008) *Guidelines for Nonlinear Analysis of Bridge Structures in California*. PEER Report 2008/03.

28. Tahouni, Sh. (2008) *Bridge Design: Reinforced Concrete, Steel and Pre-Stressed Bridges*. Tehran University Press.

29. *Linear and Nonlinear Static and Dynamic Analysis and Design of Three-Dimensional Structures*, Version (14.1.0), Computers & Structures, Inc., Berkeley, California, USA.

30. Bentz, E.C. and Collins, M.P. (2000) *Reinforced Concrete Sectional Analysis Using the Modified Compression Field Theory*.

31. Somerville, P.G. (2003) Magnitude scaling of the near fault rupture directivity pulse. *Physics of the Earth and Planetary Interiors*, **137**, 201-212.

32. Wang, J., Carr, A., Cooke, N., and Moss, P. (2003) Wave-passage effect on the seismic response of long bridges. *Pacific Conference on Earthquake Engineering*.

Appendix A

Table A1. Model input parameters obtained by fitting the analytical model to recorded near-fault ground motions [6].

No.	Location	Station	Component	A	γ	$\upsilon(^\circ)$	f_p (Hz)	t_0 (sec)
1	San Fernando, CA, USA	PCD	SN	115.0	1.6	180.0	0.680	3.00
2	Tabas, Iran	TAB	SP	104.0	2.2	180.0	0.190	12.40
3	Imperial Valley, CA, USA	E04	SN	71.0	1.9	305.0	0.225	6.10
4		E05	SN	84.0	1.9	300.0	0.255	6.60
5		E06	SN	96.0	2.1	265.0	0.260	6.35
6		E07	SN	79.0	2.1	25.0	0.275	6.10
7		EMO	SN	78.0	2.3	0.0	0.340	4.95
8	Superstition Hills, CA, USA	PTS	SN	112.0	1.8	237.0	0.445	12.295
9		ELC	SN	46.0	1.7	210.0	0.430	13.180
10	Loma Prieta, CA, USA	LPG	SN	60.0	3.0	280.0	0.310	7.600
11		STG	SN	47.0	1.9	150.0	0.270	6.500
12	Erzincan, Turkey	ERZ	SN	67.0	2.5	210.0	0.410	3.700
13	Northridge, CA, USA	JFA	SN	87.0	2.3	100.0	0.330	4.120
14		RRS	SN	142.0	1.7	20.0	0.800	2.430
15		SCG	SN	93.0	2.5	0.0	0.340	3.650
16		SCH	SN	80.0	2.3	0.0	0.330	3.770
17		NWS	SN	94.0	1.7	200.0	0.370	4.770

Table A2. Summary of earthquake events and recording station data for the near-field records set.

ID No.	Earthquake			Recording Station	Recorded Motions		Site-Source Distance
	M	Year	Name	Name	PGA_{max} (g)	PGV_{max} (cm/s)	Closest to Plane (km)
1	6.5	1979	Imperial Valley-06	El Centro Array#6	0.44	111.9	1.4
2	6.5	1979	Imperial Valley-06	El Centro Array#7	0.46	108.9	0.6
3	6.9	1980	Irpinia, Italy-01	Sturno	0.31	45.5	10.8
4	6.5	1987	Superstition Hill-02	Parachute Test Site	0.42	106.8	1
5	6.9	1989	Loma Prieta	Saratoga-Aloha	0.38	55.6	8.5
6	6.7	1992	Erzincan, Turkey	Erzincan	0.49	95.5	4.4
7	7	1992	Cape Mendocino	Petrolia	0.63	82.1	8.2
8	7.3	1992	Landers	Lucerne	0.79	140.3	2.2
9	6.7	1994	Northridge-01	Rinaldi Receiving Sta	0.87	167.3	6.5
10	6.7	1994	Northridge-01	Sylmar-Olive View	0.73	122.8	5.3
11	7.5	1999	Kocacli, Turkey	Izmit	0.22	29.8	7.2
12	7.6	1999	Chi-Chi, Taiwan	TCU065	0.82	127.7	0.6
13	7.6	1999	Chi-Chi, Taiwan	TCU102	0.29	106.6	1.5
14	7.1	1999	Duzce, Turkey	Duzce	0.52	79.3	6.6
15	7.11	1978	Tabas, Iran	TAB	0.931	122	1.2
16	6.9	1989	Loma Prieta, CA	LGP	0.605	102	3
17	6.4	1987	Superstition Hills, CA	ELC	0.358	52	10.6
18	6.55	1971	San Fernando, CA	PCD	1.22	120	3
19	6.5	1979	Imperial Valley	E04	0.3745	73.86	6
20	6.5	1979	Imperial Valley	E05	0.4481	71.18	2.7
21	6.5	1979	Imperial Valley	E06	0.4273	83.49	0.3
22	6.5	1979	Imperial Valley	E07	0.42	79.15	1.8
23	6.5	1979	Imperial Valley	EMO	0.3092	79.79	1.2
24	6.7	1994	Northridge, CA	NWS	0.3848	79.07	5.3
25	6.7	1994	Northridge, CA	SCH	0.6469	95.07	5
26	6.7	1994	Northridge, CA	JFA	0.7636	73.99	5.2
27	6.7	1994	Northridge, CA	SCG	0.7123	109.38	5.1

Table A3. Summary of earthquake events and recording station data for the far-field records set.

ID No.	Earthquake			Recording Station	Recorded Motions		Site-Source Distance
	M	Year	Name	Name	PGA_{max} (g)	PGV_{max} (cm/s)	Closest to Plane (km)
1	6.7	1994	Northridge	Beverly hills-Mulhol	0.52	63	17.2
2	6.7	1994	Northridge	Canyon Country-WLC	0.48	45	12.4
3	7.1	1999	Duzce, Turkey	Bolu	0.82	62	12
4	7.1	1999	Hector Mine	Hector	0.34	42	11.7
5	6.5	1979	Imperial Valley	Delta	0.35	33	22
6	6.5	1979	Imperial Valley	El Centro Array#1	0.38	42	12.5
7	6.9	1995	Kobe, Japan	Nishi-Akashi	0.51	37	7.1
8	6.9	1995	Kobe, Japan	Shin-Osaka	0.24	38	19.2
9	7.5	1999	Kocaeli, Turkey	Duzce	0.36	59	15.4
10	7.5	1999	Kocaeli, Turkey	Arcelik	0.22	40	13.5
11	7.3	1992	Landers	Yermo Fire Station	0.24	52	23.6
12	7.3	1992	Landers	Coolwater	0.42	42	19.7
13	6.9	1989	Loma Prieta	Capitola	0.53	35	15.2
14	6.9	1989	Loma Prieta	Gilroy Array#3	0.56	45	12.8
15	7.4	1990	Manjil, Iran	Abbar	0.51	54	12.6
16	6.5	1987	Superstition Hills	El Centro Imp. Co.	0.36	46	18.2
17	6.5	1987	Superstition Hills	Poe Road	0.45	36	11.2
18	7	1992	Cape Mendocino	Rio Dell Overpass	0.55	44	14.3
19	7.6	1999	Chi-Chi, Taiwan	CHY101	0.44	115	10
20	7.6	1999	Chi-Chi, Taiwan	TCU045	0.51	39	26
21	6.5	1971	San Fernando	LA-Hollywood	0.21	19	22.8
22	6.5	1976	Friuli, Italy	Tolmezzo	0.35	31	15.8